Title

On the origin of the gamma-ray emission from Omega Centauri: millisecond pulsars and dark matter annihilation

Journal

Journal of Cosmology and Astroparticle Physics, 2021(02)

ISSN

1475-7516

Authors

Reynoso-Cordova, Javier
Burgueño, Oleg
Geringer-Sameth, Alex
et al.

Publication Date

2021-02-01

DOI

10.1088/1475-7516/2021/02/010

Peer reviewed

On the origin of the gamma-ray emission from Omega Centauri: Milisecond pulsars and dark matter annihilation

Javier Reynoso-Cordova,[1,*] Oleg Burgueño,[1,†] Alex Geringer-Sameth,[2]
Alma X. González-Morales,[1,3] Stefano Profumo,[4] and O. Valenzuela[5]

[1] *Departamento de Física, DCI, Campus León, Universidad de Guanajuato, 37150, León, Guanajuato, México*
[2] *Department of Physics, Imperial College London, Blackett Laboratory, Prince Consort Road, London SW7 2AZ, UK*
[3] *Consejo Nacional de Ciencia y Tecnología, Av. Insurgentes Sur 1582. Colonia Crédito Constructor, Del. Benito Juárez, C.P. 03940, México D.F. México*
[4] *Department of Physics and Santa Cruz Institute for Particle Physics University of California, Santa Cruz, CA 95064, USA*
[5] *Instituto de Astronomía, Universidad Nacional Autónoma de México, A. P. 70-264, 04510, México, CDMX, México*

We explore two possible scenarios to explain the observed γ-ray emission associated with the atypical globular cluster ω-Centauri: emission from millisecond pulsars (MSP) and dark matter (DM) annihilation. In the first case the total number of MSPs needed to produce the γ-ray flux is compatible with the known (but not confirmed) MSP candidates observed in X-rays. A DM interpretation is motivated by the possibility of ω-Centauri being the remnant core of an ancient dwarf galaxy hosting a surviving DM component. At least two annihilation channels, light quarks and muons, can plausibly produce the observed γ-ray spectrum. We outline constraints on the parameter space of DM mass versus the product of the pair-annihilation cross section and integrated squared DM density (the so-called J-factor). We translate upper limits on the dark matter content of ω-Centauri into lower limits on the annihilation cross section. This shows s-wave annihilation into muons to be inconsistent with CMB observations, while a small window for annihilation into light quarks is allowed. Further analysis of ω-Centauri's internal kinematics, and/or additional information on the resident MSP population will yield much stronger constraints and shed light about the origin of this otherwise mysterious γ-ray source.

PACS numbers: 95.35.+d

I. INTRODUCTION

Omega Centauri (ω-Cen) is a globular cluster (GC) that has received significant attention over the last few decades due to its unique properties. Arguably the most massive GC in the Galaxy with a mass $\sim 10^6$ $M_\odot$ [1–4], the nature of its stellar population is a rather hotly debated topic. Previous work suggests that ω-Cen 's star formation history is quite different from that of other GCs, making it challenging to explain its stellar population as an isolated object [5–9]. ω-Cen has a high concentration of calcium and other heavy metals [10] as compared to other GCs, which can be explained by supernovae metal enrichment [11, 12]. However, ω-Cen 's present gravitational potential is not deep enough to retain the ejected material from a supernova explosion [11]. Such observations led to the hypothesis that this unique GC may be the remnant core of an ancient, tidally disrupted dwarf galaxy [5, 10, 13–24]. Unlike a typical GC, dwarf galaxies are dark matter (DM) dominated systems, as inferred from their dynamically-determined mass-to-light ratios [25]. If ω-Cen is the vestige of one of such object it must have lost most of its external DM through tidal interactions with the Milky Way since its stellar kinematics has not yet shown any strong evidence for the presence of a DM halo. The recent discovery of tidal debris spread along ω-Cen 's orbit adds evidence to this scenario [26].

The analysis of recent measurements of ω-Cen 's internal kinematics [4], using the Hubble Space Telescope (HSP) proper-motion catalogue, assuming a constant mass-to-light ratio Υ, found $\Upsilon = 2.66$. On the other hand, a value of $\Upsilon = 1.87 \pm 0.15$ was determined from stellar population-synthesis modeling [3]. Differences in mass-to-light ratios determined from the kinematics and stellar populations, could be explained due to variations in the initial mass function, or due to mass that can be attributed to the dark matter component, see the discussion in [27] for an example. Even though we do not claim here that the differences found for ω-Cen *per se* suggests the presence of a relic DM halo, it can certainly be used to derive an upper limit to the amount of DM present on it.

Dark matter is currently one of the most pressing puzzles in physics and astronomy, making up nearly 26% [28] of the total energy density in the Universe. With no non-gravitational signals detected so far, its fundamental nature remains a mystery. One distinct possibility is that particle dark matter annihilates with its anti-particle to produce stable Standard Model particles, including photons. The typical energies of such photons would then be around and below the dark matter particle mass. For weak-scale dark matter particles, this would entail the production of gamma rays, a possible tell-tale sign of

* reynosoj@fisica.ugto.mx
† olegs@fisica.ugto.mx

dark matter annihilation.

In 2010 the Fermi Large Area Telescope (Fermi-LAT) collaboration [29–31] published an analysis of γ-ray emission from a collection of Milky Way GCs. They reported a non-zero flux from some GCs including ω-Cen [32]. The conventional explanation is that the emission is due to populations of millisecond pulsars (MSPs) within the GCs. These ancient, short-period pulsars are thought to be "recycled" neutron stars "spun up" through the loss of orbital angular momentum to their binary companion. For ω-Cen , the study concluded that a population of 19 ± 9 MSPs are needed to reproduce the data, assuming all MSPs have the same values for emissivity power and efficiency [32]. Recent X-ray experiments show there are about thirty candidate MSPs in ω-Cen [33], but none of these has yet been confirmed as a pulsar.

The search for high-energy particles, in particular γ-rays, produced by DM annihilation (or decay) in astrophysical systems has been extensively pursued over the last decade (for a review see [34, 35]). Such an astronomical detection would shed light on the fundamental nature of DM and particle physics beyond the Standard Model. Given that ω-Cen could be the remnant core of a disrupted galaxy and actually have a (subdominant) DM component, it is timely to explore under which conditions DM annihilation can reproduce Fermi-LAT observations. This can impose important constraints on the parameter space of DM particle properties as well as on the distribution of DM within ω-Cen itself, e.g. [36, 37].

In this work we analyze ~ 9.5 years of γ-ray observations by Fermi-LAT from the direction of ω-Cen . Data reduction and analysis methods are outlined in Sec. II; In Sec. III we present the details, and the assumptions we make, for the MSP and DM scenarios for the origin of the γ-ray emission; in Sec. IV we describe the results of the analysis in the two scenarios of MSP and DM and we also provide an extended discussion on the selection of the annihilation channels and possible constraints on the thermal averaged cross section. Finally, we discuss our results and summarize our findings in Sec. V.

We emphasize that we do not claim here that DM annihilation is the most viable mechanism to explain the observed γ-ray emission from ω-Cen . Our goal is, rather, to place conservative constraints on DM properties, including its abundance, in order to be compatible with observations. Finally we intend to compare this alternative explanation against a model where MSPs give rise to the γ-ray emission.

II. DATA SELECTION AND ANALYSIS

In this section we explain in detail the procedure used to reduce the data as well as the methodology to analyze it. The main purpose of the Fermi-LAT [29–31] is to observe energetic γ-rays coming from Galactic and extragalactic sources whose energy lies in the range from ~ 100 MeV up to $\gtrsim 300$ GeV. As stated before, our object of study is the globular cluster Omega Centauri (ω-Cen), with coordinates: 201.6970 RA and -47.4795 DEC according to the Fourth Fermi Gamma-ray Source Catalog (4FGL) catalog [38] (2.89×10^{-5} deg from ω-Cen 's position according to [39]). Using v10r0p5 of the Fermi Science Tools [1], we select ~ 9.5 years of LAT data (between MET 239557417s and 574181612s). We adopt a region of interest (ROI) of 0.2 deg radius around the position of ω-Cen in the 4FGL and select all Pass 8R3 Source events (`evclass=128` and `evtype=3`), in the $0.2 - 50$ GeV range within the ROI using `gtselect` with a maximum zenith angle of 90 deg. We use the standard filter `"DATA_QUAL> 0 && (LAT_CONFIG== 1)"` in `gtmktime`, we use `dcostheta=0.025` and `binsz=1` in `gtltcube`, and `theta=300` and `thetamax=1 deg` in `gtpsf` to obtain the exposure, ϵ, (observation time times effective area) and point spread function, PSF, both functions of energy. We extract the measured energy spectrum in 15 equally log-spaced energy bins between 0.2 and 50 GeV using `gtbin` with the PHA1 algorithm.

We analyze the data by fitting proposed models to the observed photon flux, see for instance [40–42] in the context of LAT data. Since the the photon count coming from ω-Cen is low the observations are most accurately described by a Poisson likelihood, defined by

$$\mathcal{L} = \prod_i \frac{e^{-\lambda_i} \lambda_i^{d_i}}{d_i!}, \tag{1}$$

where the product is over energy bins i, d_i is the number of counts observed in each bin, and λ_i is the corresponding model prediction.

There is one known gamma-ray source (4FGL J1328.5-4727) within 1° of our target according to the 4FGL[2] (besides the source associated with ω-Cen itself). According to the 4FGL, its energy spectrum corresponds to a power law with no cutoff. To take into account its contribution to the total number of events we will include it in the likelihood at the catalog position and use several nuisance parameters to describe its energy spectrum.

The general form for the model is given by

$$\lambda = M(E, \Theta) + S(E, \eta) + B(E), \tag{2}$$

where M corresponds to the emission from ω-Cen (to be defined in section III A for MSP, and III B for DM). S corresponds to the nearby point source for which the flux is modeled with a simple power law with no cut-off: $d\phi/dE = N_s(E/E_p)^{-\alpha_s}$. Here N_s and α_s are the normalization and the spectral index, respectively, and will be treated as nuisance parameters that we marginalize

[1] https://fermi.gsfc.nasa.gov/ssc/data/analysis/software/

[2] In the previous 3FGL catalog [43], there were two nearby sources within 1 degree of ω-Cen . We report the analysis with only the one source present in the latest catalog. However, our conclusions are robust to the inclusion of the other one.

over (E_p is an arbitrary reference energy which we set to 4726.70 MeV according to the 4FGL catalog). To obtain the number of events contributed by this point source, we integrate the energy flux within the energy bins limits, as well as integrating the PSF (centered on the point source) over the ω-Cen ROI as specified in Eq. (A2).

Finally $B(E)$ corresponds to the diffuse and isotropic background components. We adopt the Fermi collaboration model[3] consisting of interstellar galactic emission[4] and an isotropic component[5]. The prediction $B(E)$ within each energy bin is found by multiplying the sum of these two component spectra by the LAT exposure and the solid angle of the ROI and then integrating over the energy bin.

With the likelihood defined, we perform a Monte Carlo Markov Chain (MCMC) analysis to generate posterior distributions for the model parameters. We use flat priors for parameters describing the emission from ω-Cen , whereas Gaussian priors are used for the those describing the nearby source. These are specified in section IV. For the MCMC we use the `emcee` package, which is an affine invariant ensemble sampler [44]. Our base setup for the MCMC is to use 200 walkers with 1500 steps and a burn-in phase of 500 steps. To check for convergence we performed two checks: (a) we doubled the number of steps with a fixed number of walkers; (b) we doubled the number of walkers with the number of steps fixed as recommended by the authors of the sampler to reduce the noise in the chains. In both tests we find similar results to the base setup. Finally, to compare the different models we use the Akaike Information Criterion, $AIC = -2k - 2\ln(\mathcal{Z})$, where k is the number of free parameters in the model and $\mathcal{Z}$ is the evidence. Smaller values of the AIC indicate the model is a better fit to the data, after penalizing for the number of free parameters in the model. In this case evidences were computed using the `pymultinest` code [45, 46], that uses a nested sampling algorithm, for which one of the main features is to compute the evidence. The use of `multinest` also served as a cross check of the `emcee` results.

III. POSSIBLE EXPLANATIONS FOR THE ω-CEN OBSERVED γ-RAYS EVENTS

A. Milisecond Pulsars

Thus far, the only hypothesis explored to explain the observed flux of γ-rays from ω-Cen is that they originate from MSPs [32, 41, 42]. In this scenario the photon flux is commonly modelled with an exponentially cut-off power law given by

$$\frac{d\phi}{dE} = N_0 (E/\mathrm{MeV})^{-\Gamma} \mathrm{e}^{-E/E_{\mathrm{cut}}}, \tag{3}$$

where N_0 is the normalization, Γ is the spectral index and E_{cut} is the energy cutoff. Those three are the free parameters to be fitted in our the analysis, together with two nuisance parameters associated to the nearby point source. To compute the predicted number of events detected in an energy bin with limits E_1 and E_2 we need to include information from the instrument response, namely the exposure ϵ and the point spread function (PSF) which gives the probability that a photon originating from ω-Cen is reconstructed within our defined ROI. Since these two quantities are energy-dependent, the expected number of events for the i-th energy bin is given by

$$M(E_i) = \int_{E_i}^{E_{i+1}} \int_{\Delta\Omega} d\Omega \, \epsilon(E) \mathrm{PSF}(\mathrm{E}, \Theta) \frac{\mathrm{d}\phi}{\mathrm{dE}}. \tag{4}$$

Note that the above equation takes ω-Cen to be a point source of γ-rays. This is a valid assumption as the scale radius of the emission ought to be of the order the half-light radius [17], which is less than the width of the PSF ($\gtrsim 0.2^\circ$) at the energies relevant to our analysis.

Once the model parameters are determined, by means of the MCMC using the likelihood defined in Sec. II, the next step is to compute the associated number of MSPs giving rise to the emission. Following [32], the number of MSPs is approximated by

$$N_{\mathrm{MSP}} = \frac{L_\gamma}{\left\langle \dot{E} \right\rangle \eta}, \tag{5}$$

where L_γ is the isotropic luminosity, η is the estimated average spin-down to γ-ray luminosity conversion efficiency and $\langle \dot{E} \rangle$ is the average spin-down power. We adopt the values of $\langle \dot{E} \rangle$ and η from Ref. [32]. The simplest approach is to approximate L_γ directly from the observed energy flux S and the distance to the source d [32],

$$L_\gamma = 4\pi S d^2. \tag{6}$$

Note that Ref. [41] estimates the number of MSPs in a globular cluster by correlating the number of binary systems that can be formed given a stellar density and γ-ray luminosity, whereas in Ref. [42] a correlation between the X-ray and γ-ray flux is used in order to compute how many MSPs could contribute to the γ-ray flux. These studies argue that the naive way to compute the number of MSPs used by [32] can lead to a wrong answer since, for a globular cluster, the γ-ray emission could be due to one really luminous MSP or the sum of several fainter ones. The details on how the MSPs are contributing to the γ-ray photon flux could lead to important differences in the analysis, specially when multiple components of the γ-ray source are considered. See for instance the analysis by

[3] `http://fermi.gsfc.nasa.gov/ssc/data/access/lat/BackgroundModels.html`
[4] `gll_iem_v07.fits`
[5] `iso_P8R3_SOURCE_V2_v1.txt`

[37] and [36] on the 47 Tuc GC, which we discuss in section V. As mentioned earlier there are ~ 30 sources with X-ray-MSP-like emission in ω-Cen [33], but there is no confirmation with radio observations that these sources are pulsars. Therefore, we consider the simple approach given by Eq. (6) to be sufficient to obtain the order of magnitude of the number of MSPs required to explain ω-Cen 's observed γ-ray photon flux.

B. Gamma rays from annihilating dark matter

As stated in Sec. I, one of our goals is to explore the possibility that ω-Cen 's energy spectrum is produced by the annihilation of DM into Standard Model particles. In this case the photon flux from ω-Cen is given by[6]

$$\frac{d\phi}{dE} = \frac{1}{8\pi} J_{\Delta\Omega} \frac{\langle\sigma v\rangle}{m_\chi^2} \frac{dN}{dE}, \tag{7}$$

where $\langle\sigma v\rangle$ is the thermal averaged annihilation cross section, m_χ is the dark matter particle mass, dN/dE is the photon spectrum produced for each annihilation, and $J_{\Delta\Omega}$ is the so-called astrophysical J-factor . The J-factor encodes information about the DM density distribution within ω-Cen . It is the integral over a solid angle $\Delta\Omega$ of the J-profile $dJ/d\Omega$, which determines the spatial morphology of γ-ray emission from DM annihilation. The J-profile is defined as the integral of the square of the dark matter mass density $\rho(r)$ along a line of sight that makes an angle θ with the direction toward the center of ω-Cen (e.g. [47]):

$$\frac{dJ}{d\Omega}(\theta) = \int \rho^2(r(\theta,\ell))d\ell, \tag{8}$$

$$J_{\Delta\Omega} = \int_{\Delta\Omega} \frac{dJ}{d\Omega} d\Omega. \tag{9}$$

One common approach is to use the observed stellar or gas kinematics to constrain the DM density distribution and then use this density profile to determine the J-factor for a given target. For nearby dwarf spheroidal galaxies this is usually done by fitting the free parameters of a proposed DM density profile using the Jeans equation (e.g. [48, 49]). For Galactic Center studies, the proposed Milky Way DM density profile is normalized so that it matches the inferred DM density in the solar neighborhood, and is then extrapolated to the very inner regions [50, 51]. In dwarf spheroidals, propagating the uncertainties in the observed kinematics and the influence of different DM and velocity anisotropy profiles have yielded relatively constrained estimates for the J-factor [e.g. 47, 49, 52].

[6] Notice that Eq. (7) assumes that the dark matter is its own antiparticle; if this is not the case, and there is an equal number of dark matter particles and antiparticles, an additional factor 1/2 would be needed.

We are not aware of any previous work pursuing this kind of analysis for the case of ω-Cen , i.e. there are no specific constraints to the DM density profile that could be associated with it. Performing a Jeans (or similar) analysis of ω-Cen kinematics including a DM component is by itself an interesting possibility which, however, is out of the scope of this paper. For this work we use available information on the different estimates of ω-Cen 's mass-to-light ratio Υ to set an upper limit on the dark matter mass possibly contained within ω-Cen 's half-light radius, r_h, and use that to pinpoint a reasonable range for the J-factor . We spell this out next. Using population-synthesis models to compute stellar properties, a mass-to-light ratio of $\Upsilon_{\rm syn} = 1.87 \pm 0.15$ was found in Ref. [3]. On the other hand, in Ref. [2], spherical, non rotating, dynamical models with constant mass-to-light ratio were fitted to the most recent Hubble Space Telescope proper motions [53], finding $\Upsilon_{\rm dyn} = 2.66 \pm 0.04$. The tension between these two values might be due to differences in the initial mass functions (IMF) [2]. However the possibility that a dark matter component can explain the difference between dynamical and stellar mass-to-light estimates has not been discussed. We do not attempt to demonstrate here that the difference is minimized by including DM as another $\omega-$cen component, but merely use the difference between the two determinations of Υ to set a possible maximum value for the DM contribution to the mass.

Following Ref. [54], we compute the stellar mass using a cylindrical stellar density profile given by a Gaussian decomposition:

$$\rho_*(z,R) = \sum_j^M \frac{M_j}{(2\pi\sigma_j^2)^{3/2} q_j} \exp\left[-\frac{1}{2\sigma_{\rm j}^2}\left(\mathrm{R}^2 + \frac{\mathrm{z}^2}{\mathrm{q}_{\rm j}^2}\right)\right], \tag{10}$$

where M_j are the different mass components, σ_j controls the extent along the major axis, and q_j is the projected flattening. We set all parameters as in [54]. Using this decomposition we compute the stellar mass present in ω-Cen for the two Υ values described above. Then we compute the difference between these two values which is approximately $\delta M(r_h) = 1.01 \times 10^5\,\mathrm{M}_\odot$, where r_h is the ω-Cen half light radius equal to 7 pc [54]. We take $\delta M(r_h)$ as the maximum total mass within r_h that could be attributed to a DM halo. Note that according to the simulations of [55], the dark matter mass that could remain in a ω-Cen like object after a tidal disruption, assuming ω-Cen is the remnant of a dwarf galaxy, would be $M_{DM} \sim 4 \times 10^5 M_\odot$. Since to date there are no observational constraints on ω-Cen 's DM component we can only point out that the total mass limit we adopt is similar to what is expected from predictions based on these numerical simulations.

To model the DM density in Eq. (8), we adopt a gen-

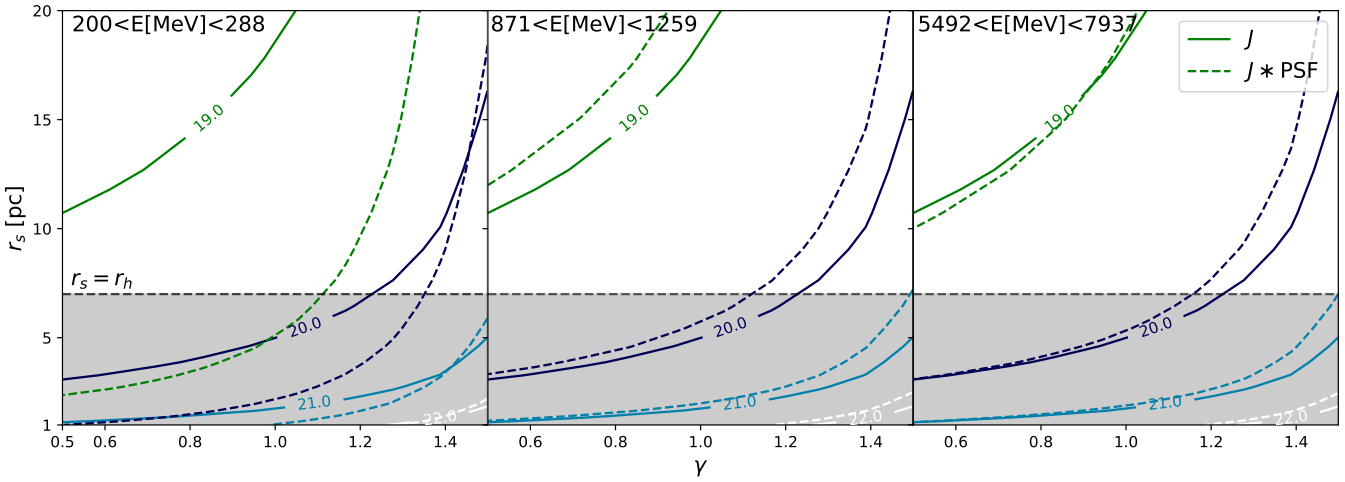

FIG. 1. Comparison between the J-factor (Eq. 8), in $\log_{10}$ scale, which is constant for all energy bins (solid lines) and the convolution of the J-factor with the PSF weighted by the PSF (Eq. 12, dashed lines), as a function of the scale radius and inner slope γ of the DM density profile (Eq. (11)). The three panels show results for three different energy bins. Shaded region below the $r_s = r_h$ would correspond to what we consider non-physical J-factor values if ω-Cen is the remnant of a disrupted galaxy.

eralized Navarro-Frenk-White density profile;

$$\rho(r) = \frac{\rho_s}{\left(\frac{r}{r_s}\right)^{\gamma}\left(1+\left(\frac{r}{r_s}\right)\right)^{(3-\gamma)}}, \tag{11}$$

where ρ_s and r_s are the characteristic density and scale radius respectively.

Further, we make some assumptions on the properties of the DM halo. A simple picture of ω-Cen being the remnant of a disrupted galaxy would require the scale radius to be larger than the observed luminous half mass radius, otherwise the stellar component would not survive the disruption. On the other hand, one could extrapolate mass-concentration relations such as the one proposed in Ref. [56], which seems to hold even for small halos [57], and compute the scale radius for a halo mass of $10^6 M_\odot$, which results in a few parsecs. Therefore we can safely assume the scale radius to be larger or of the order of $r_{\rm h}$. For a given r_s and γ we determine ρ_s so that the enclosed mass within the half-light radius is equal to the DM mass limit found from the difference between the values of the mass-to-light-ratios computed above: $M_{\rm DM}(r_h) = \delta M(r_h) = 1.01 \times 10^5\,{\rm M}_\odot$.

It is important to take into account that, just as in the calculation for the number of events using the MSP model, we must include the information regarding the instrument response. The case of DM is trickier than for MSPs since the angular extent of the dark matter emission profile may be comparable to or broader than the PSF. The way to incorporate the PSF information is through its convolution with the J-profile so that the observed number of events is given by

$$\frac{dN}{dE}_{\rm observed} = \frac{1}{8\pi}\frac{\langle\sigma v\rangle}{m_\chi^2}\frac{dN}{dE}\int_{\Delta\Omega} d\Omega \left(\frac{dJ}{d\Omega} * {\rm PSF}\right)(E,\theta). \tag{12}$$

Over a small patch of sky the integral over solid angle becomes a 2D rectangular integral which can be performed using a zeroth order one-dimensional Hankel transform [47]. For this we use the python package *mcfit* which uses the FFTlog algorithm [58]. We give the details of this procedure in Appendix B.

Formally, the density profile parameters r_h and γ should be sampled by the MCMC, but this would involve performing the convolution on every MCMC step, which would be computationally expensive. As a simpler approach, we will use a single value of the J-factor for all energy bins which is then multiplied by the energy-dependent PSF. Then we will give an estimate of the error that we might be introducing by this approximation. In Figure 1 we show, for three energy bins, how the convolution of the J-profile with the PSF integrated over the ROI (dashed lines), and divided by the integrated PSF, approaches to the unconvolved J-factor for high energies (solid lines) and substantially differs for low energies (dashed lines). That is, for the high-energy bins the equality

$$J_{\Delta\Omega} = \frac{\int_{\Delta\Omega} d\Omega \left(\frac{dJ}{d\Omega} * {\rm PSF}\right)(E,\theta)}{\int_{\Delta\Omega} d\Omega {\rm PSF}(\theta)} \tag{13}$$

holds. The relatively large difference, between the convolved and unconvolved J-factor in the low energy bins will lead to different results specifically for the analysis of the $\bar{q}q$ channel. As we discuss in Sec. V B, the approximation made does not have a great impact on our

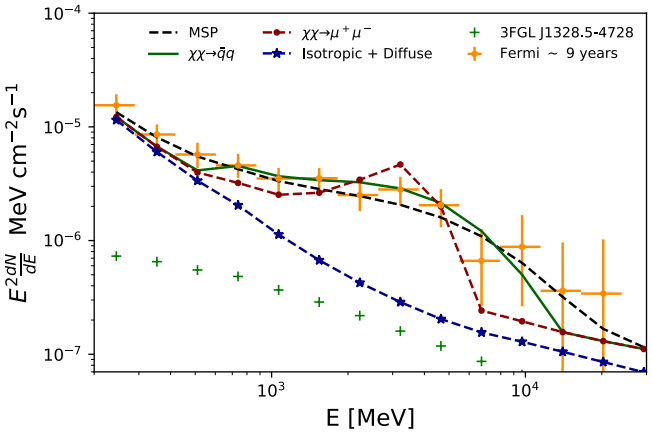

FIG. 2. ω-Cen energy flux (yellow dots) as observed with the Fermi-LAT corresponding to $\sim$ 9 years. Dashed black line shows the total flux predicted by the Millisecond Pulsar model (section IV A). Green solid line and point-dashed line correspond to total flux for the DM models annihilating into light quark-antiquark $q\bar{q}$ and muon-antimoun $\mu^+\mu^-$, respectively, as described on IV B. For this plot we used the median values of the fitted parameters shown in Figure 3. Also shown for reference is the background contribution to the total flux.

Γ	$\log_{10}(E_{cut})$	$\log_{10}(N_0)$	N_{MSP}
$1.58^{+0.26}_{-0.26}$	$3.55^{+0.18}_{-0.14}$	$-6.89^{+0.71}_{-0.85}$	$31.78^{+18.77}_{-7.97}$
	$\log_{10}(N_S)$	α_s	AIC
	$-11.43^{+0.08}_{-0.10}$	$2.70^{+0.13}_{-0.13}$	20.3

TABLE I. Median values obtained by the inference for the MSP model parameters (see figure 3) and the corresponding Akaike information criterion parameter (AIC). The error bars for all the parameters are at a 95% confidence.

conclusions. We also note that the analysis of [59] prefers a point-source model of ω-Cen to an extended one, which is also consistent with our approximation of using a constant J-factor for all energy bins.

IV. ANALYSIS AND RESULTS

Using the models for γ-ray emission from ω-Cen described in Sections III A and III B, we now proceed to analyze the data using the statistical methods specified in Section II.

A. MSPs

We model MSP emission in ω-Cen as a power law spectrum with exponential cut-off given by Eq. (3) with three free parameters: N_0, Γ, $E_{\rm cut}$. The two nuisance parameters N_s and α_s describe the energy spectrum of the nearby source. For the ω-Cen parameters we use flat priors over the following ranges:

- $0 < \Gamma < 3$,
- $2 < \log_{10}(E_{\rm cut}/{\rm MeV}) < 8$,
- $-18 < \log_{10}(N_0/{\rm MeV}) < 0$.

We adopt Gaussian priors for N_s and α_s based on the best fitting values and error bars reported in the 4FGL catalog [38]:

- $\frac{N_s}{10^{-14}} = 3.81 \pm 0.39\ {\rm MeV}^{-1}$
- $\alpha_s = 1.98 \pm 0.07$

The results for the fit are shown in Figure 3, where we have added a last panel for the derived quantity of interest, the number of MSPs in ω-Cen. The flux from the MSP contribution that corresponds to the median values of the posterior is shown in Figure 2 (black dashed line). Also shown are the fluxes from the nearby source and the background components (green and blue symbols respectively). In Figure 3 the shaded gray region in the $N_{\rm MSP}$ panel corresponds to the range of expected number MSPs reported by Ref. [32]. We can see those results more or less agree with our finding, although the distribution peaks at a slightly higher value, and has a long tail towards a high number of MSP.

B. Dark Matter

Under the dark matter annihilation scenario, the shape of the observed energy spectrum is determined by the mass of the DM particle and the model for final state of the annihilation. There exists some theoretical motivation for considering heavy fermion pairs as the dominant annihilation final state, based upon arguments such as helicity suppression (as in the case for Majorana fermion dark matter, which includes the supersymmetric neutralino [60]) or considering scalar mediators, typically featuring Yukawa-like interactions with fermions (see e.g. [61–64]). However, since here we intend to fit for a γ-ray spectrum whose features indicate quite clearly a low-mass dark matter particle, it would be inappropriate to consider heavy fermions, such as top and bottom quarks, as well as pair-annihilation to gauge or Higgs bosons. Therefore we focus on the following final states: muon-antimuon ($\mu^+\mu^-$) and light quark-antiquark ($\bar{q}q$) pairs.

To compute the number of events for these specific annihilation channels we use the following spectra.

- Muons: $\frac{dN}{dy} = \frac{\alpha}{\pi}\left(\frac{1-(1-y)^2}{y}\right)\left(\ln\left[\frac{s(1-y)}{m_\mu^2}\right] - 1\right)$, where $y = E/m_\chi$, α is the fine structure constant, s is the center of mass Mandelstam variable and m_μ is the muon mass. This corresponds to the use of the Altarelli-Parisi splitting function (see e.g. [65]), which is appropriate as long as the center of mass

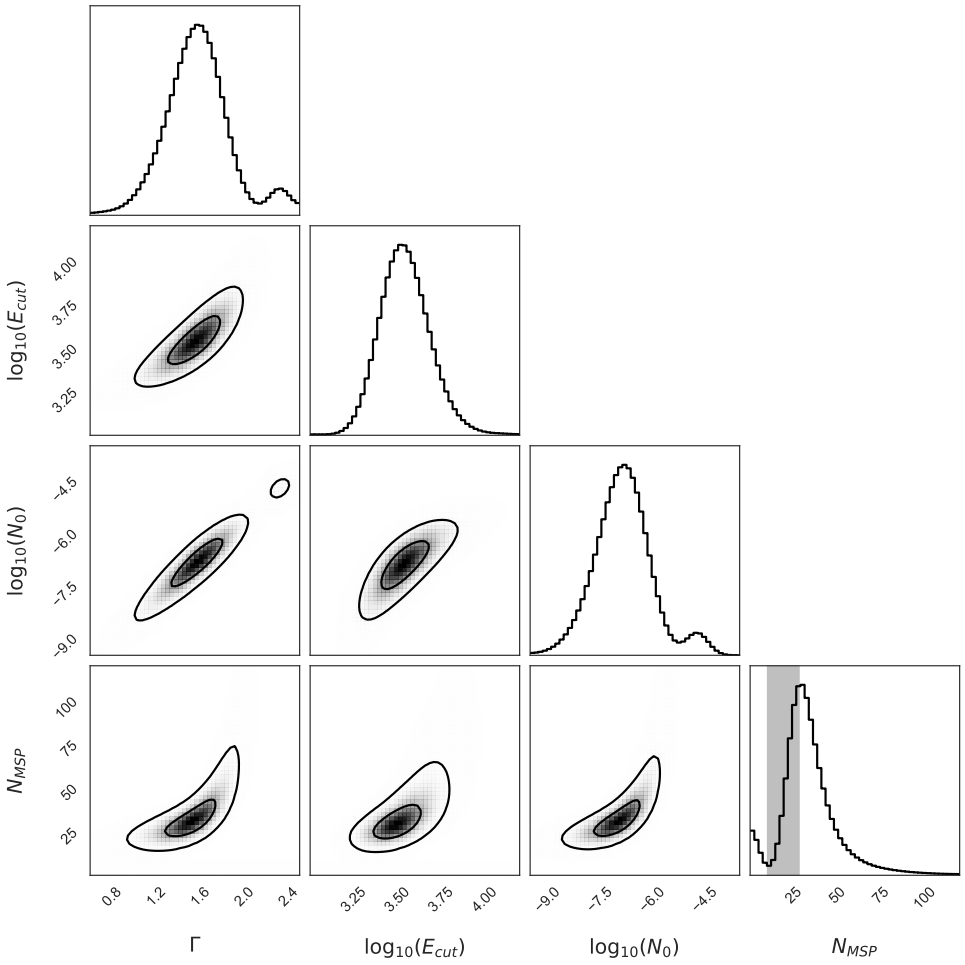

FIG. 3. Posterior probability distribution for the slope Γ, energy cut E_{cut}, and normalization N_0, that define the flux model for the millisecond pulsar hypothesis (Eq. 3). The derived number of millisecond pulsars N_{MSP} has been added at the last row. The contours corresponds to the $1-$ and $2-\sigma$ confidence for our analysis, while the shaded region in the marginalized posterior for the number of MSP corresponds to the 95% confidence from the Fermi result [32].

energy is much larger than the lepton mass, as is definitely the case for the range of masses of interest to us.

- Light quarks: $\frac{dN}{dE} = \alpha_1 \frac{E}{m_\chi} \left(\frac{E}{m_\chi}\right)^{-3/2} e^{-\alpha_2 E/m_\chi}$, which is a good approximation to simulated γ-ray spectra, with $\alpha_1 = 0.95$ and $\alpha_2 = 6.5$ [48, 66].

Before detailing the MCMC analysis for these annihilation channels we summarize existing constraints. First, for s-wave annihilation, there are strong constraints on DM with particle mass from 1 MeV up to 1 GeV coming from the angular power spectrum of the Cosmic Microwave Background (CMB). An extra injection of energy from DM annihilation can ionize the neutral hydrogen during the Dark Ages, changing the effective free electron fraction left after recombination, and thus affecting the power spectrum. A thorough analysis of CMB data leads to the constraint [28]

$$f_{\rm eff} \frac{\langle \sigma v \rangle}{m_\chi} < 3.5 \times 10^{-28}\,{\rm GeV}^{-1}{\rm cm}^3{\rm s}^{-1}, \qquad (14)$$

where $f_{\rm eff}$ is the effective efficiency function which quantifies the total amount of deposited energy in the hydrogen gas. While $f_{\rm eff}$ is redshift-dependent, it was shown that the effect on the power spectrum is the same if we consider an effective value at $z \sim 600$ [67]. We used a value of $f_{\rm eff} = 0.3$ for both channels, as found in [67]. From Eq. 14 we obtain an exclusion limit in the mass vs cross-section plane that is independent of the ω-Cen γ-ray analysis. This corresponds to the solid black line in Fig. 5. We also show for reference the expected thermal averaged DM cross-section as a function of the particle mass that would lead to a correct relic density for a weakly interacting massive particle (WIMP), as computed by [68].

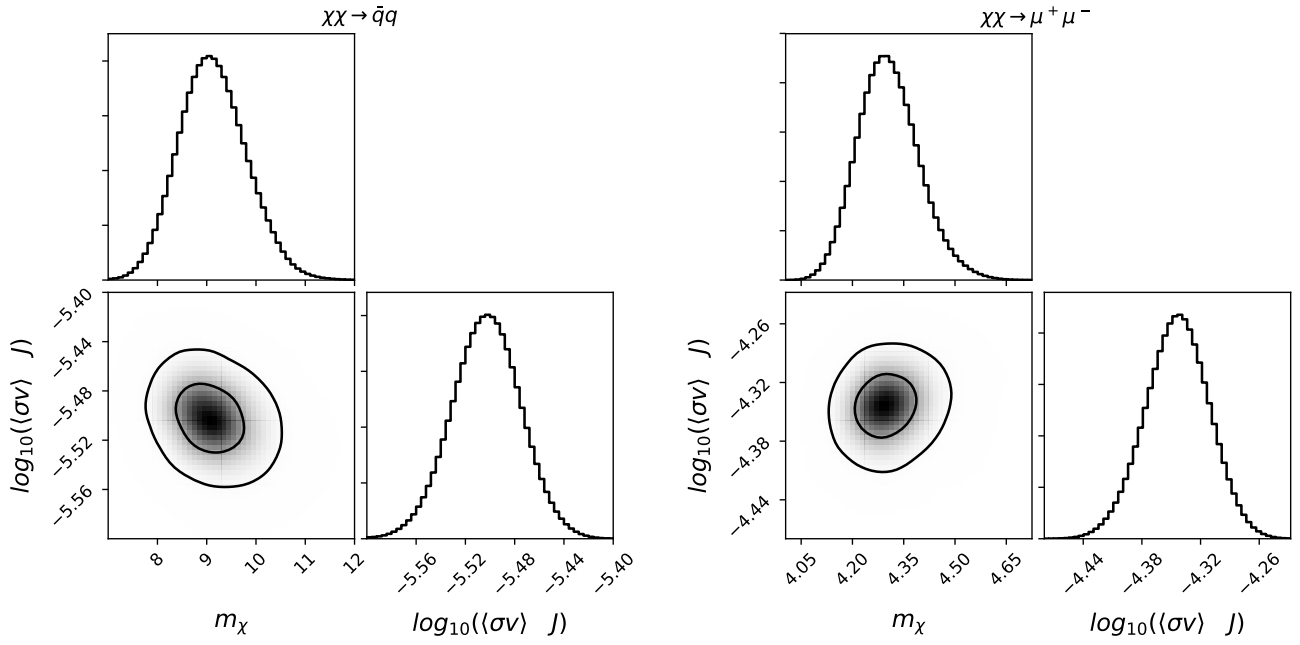

FIG. 4. Posterior probability distribution for the mass of the DM particle and $\langle\sigma v\rangle J$, for the (a) $\bar{q}q$ and (b) $\mu^+\mu^-$ annihilation channels.

To proceed further with the dark matter MCMC analysis we need to set priors for the DM mass and cross section. For the DM mass we choose a wide range that encloses the energies where the γ-ray flux is observed using the aforementioned constraints. On the other hand, whether or not we use an energy-bin dependent J-factor or a constant one in our model (Eq. 12), it is clear from Eq. 7 that there is a degeneracy between the J-factor and the cross section. When using a constant value for J, we can combine the two into a single parameter $\langle\sigma v\rangle J$. The prior on this parameter combination is not so evident. By choosing a $\log_{10}(J/\mathrm{GeV^2cm^{-5}}) = 21$, which we find to be a plausible maximum value for ω-Cen based on Figure 1, we consider a prior for the cross section in the range $10^{-31} < \langle\sigma v\rangle/\mathrm{cm^3s^{-1}} < 10^{-21}$. This would result in a range of $-10 < \log_{10}(\langle\sigma v\rangle J) < 0$. For smaller values of the J-factor, the limits of the $\langle\sigma v\rangle J$ product would be highly constrained by the CMB. With this estimate we chose a large enough prior to include a wide parameter space in the $\langle\sigma v\rangle J$ Vs mass plane:

- $0.5 < m_\chi/\mathrm{GeV} < 20$,
- $-20 < \log_{10}(\langle\sigma v\rangle J/\mathrm{GeV^2cm^{-2}s^{-1}}) < 0$,

For the nuisance parameters of the nearby source we used the same Gaussian priors as in the MSP case. In Figure 4 we show the results of the MCMC for the $\mu^+\mu_-$ and $\bar{q}q$ annihilation channels.

In Figure 5 we present the CMB constraints (black solid line), the relic density (black dashed line), and the results of the MCMC analysis (gray vertical shaded region), where the lower limit on $\langle\sigma v\rangle$corresponds the reference value of $\log_{10} J = 21$. As we can see, for our choice of the J-factor, annihilation into muons is excluded by Planck constraints, in the s-wave approximation, whilst the case of $\bar{q}q$ shows a small allowed window. A better determination of the J-factor will help reduce further the allowed parameter space. On the other hand, this could also be interpreted as an upper limit for the J-factor for a given $\langle\sigma v\rangle$.

As we claimed in Section III B, the formal way to proceed in the analysis would be to include the convolution of the PSF with the J-factor. This can be done by introducing such computation into the MCMC, leading to an exploration of a six-dimensional parameter space, the thermal averaged cross section $\langle\sigma v\rangle$, the DM density profile slope γ, the scale radius r_s, the particle mass

	$\boldsymbol{\mu^+\mu^-}$	$\boldsymbol{\bar{q}q}$
$\boldsymbol{m_\chi}$	$4.30^{+0.09}_{-0.08}$	$9.10^{+0.69}_{-0.62}$
$\boldsymbol{\log_{10}(\langle\sigma v\rangle\, J)}$	$-4.34^{+0.03}_{-0.03}$	$-5.50^{+0.03}_{-0.03}$
AIC	179.4	47.4

TABLE II. Median values found by the parameter inference for two different dark matter annihilation channels (see figure 4) and the corresponding Akaike information criterion parameter (AIC). The error bars are at a 95% confidence.

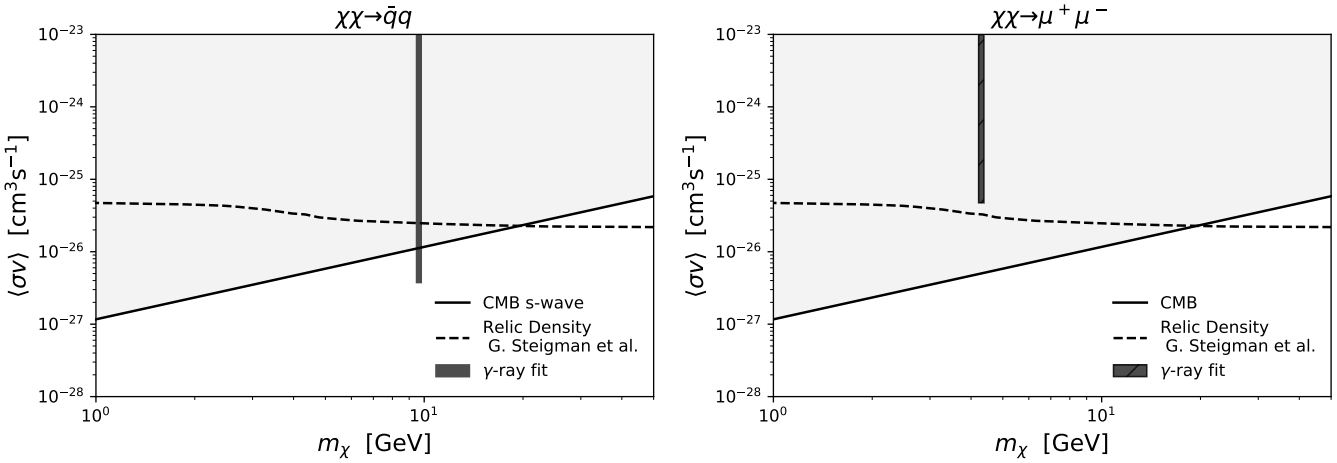

(a) (b)

FIG. 5. (a) Cross-section vs mass parameter space for DM annihilating into $\bar{q}q$ and $\mu^+\mu^-$. The dark gray vertical bar represents the 95% confidence region that explains the observed γ-ray flux. The lower edge of the bar corresponds to our estimated maximum value of the J-factor , see section III B for more details. The light gray shaded region is excluded by CMB observations (Eq. (14)). The dashed black line corresponds to the parameters that account for the total relic density. (b) Same as (a) but for DM annihilating into $\mu^+\mu^-$. In this case there is no plausible J-factor for ω-Cen that can simultaneously explain the γ-ray emission while evading the CMB constraint.

m_χ, and the two nuisance parameters associated to the nearby source. The computation of the aforementioned convolution is computationally demanding, but the actual limitation is that there is a clear degeneracy between the first three parameters. Therefore, in this work we argue that using a constant J-factor multiplied by the PSF, instead of the convolution will not alter our conclusions. As seen on Figure 1, the convolution for the higher energy bins approaches the value the non-convolved J-factor . In order to quantify the error introduced by taking a constant J-factor we took a value of $r_s = 7$ pc and $\gamma = 0.5$, computed the convolution for all energy bins, and performed the MCMC analysis over the rest of the parameters ($\langle\sigma v\rangle$, m_χ, N_s and α_s). We then compared the result with an identical procedure but fixing the J-factor to the non-convolved value for this combination of r_s and γ, $log_{10}(J) = 19.3$. We found that for $\bar{q}q$ the value of the inferred DM particle mass changes approximately $\sim 17\%$, while in the case of DM annihilating into $\mu^+\mu^-$ leaves the posterior unchanged. This can be attributed to the fact that the muon spectrum does not contribute strongly to the first energy bins, which have the largest discrepancy once the convolution is taken into account. In both channels the posteriors on $\langle\sigma v\rangle$are unaffected.

V. DISCUSSION

The motivation for this work is connected to the following observations:

(i) Given that ω-Cen 's formation is not entirely understood and that its present-day properties (such as metallicity) differentiate it from other GCs, it is possible that it is the remnant of a dwarf galaxy whose DM halo has been tidally disrupted [5, 10, 13–24].

(ii) Recent studies on ω-Cen 's internal kinematics suggest a larger mass-to-light ratio than expected from a stellar population analysis.

(iii) There is a well-identified γ-ray emission associated to it that so far cannot be definitively identified with known astrophysical objects, MSPs in particular.

Under these premises, we studied ω-Cen by fitting the γ-ray observed flux using two different models for its origin: unresolved MSPs and DM annihilation.

A. MSP

In the MSP scenario the quantity of interest is the number of MSPs inferred from the observed flux. Taking a simple approach, we concluded that a median value of ~ 30 MSPs are needed to explain the observed γ-ray emission, slightly higher than the expected number reported in [32]. This can be understood as current data indicates a higher energy cut off $E_{\rm cut}$ and harder spectral index Γ than reported in Ref. [32]. Nonetheless, the number of MSPs obtained here is consistent with the previous work of [59] who estimated the number using a similar approach to [32]. However, it has been discussed whether the estimate of the MSP population computed through Eq. (4) is reliable [42]; it could be that the luminosity of ω-Cen comes from a single very luminous pulsar or it could be the contribution of many fainter ones. The fact that there are ~ 30 MSP candidates [33] in X-ray points

to the plausible explanation of multiple MSP that also produce the γ-ray emission. With stringent constraints on the number of MSPs a deeper analysis on the luminosity function will be needed.

B. Dark Matter

Another possible scenario is that ω-Cen is the remnant of a dwarf galaxy, leading to the possibility that dark matter makes a (subdominant) contribution to ω-Cen 's mass. In this work we make a first attempt to use the observed γ-ray flux associated with ω-Cen to constrain the DM particle properties, and overall DM content itself. Given the energy range of the observed flux, we explored the possibility of it being produced by dark matter particles annihilating into $\mu^+\mu^-$ and $\bar{q}q$. For the analysis we treated the product of the astrophysical J-factor and the thermal averaged cross section as a free parameter $J\,\langle\sigma v\rangle$ along with the DM particle mass m_χ. The constraints on such parameters, found on the MCMC analysis, are reported in Table IV B. Figure 5 summarizes our results.

With the posteriors in hand, we compare the analysis results with current DM annihilation constraints. In Figure 5, the light shaded region corresponds to the thermal-averaged cross section values that are excluded by the latest Planck CMB constraints (for s-wave annihilation). The dark gray vertical band corresponds to the allowed region at the 95% confidence level, for the DM mass, found in this work. The lower limit on the cross section is set by the largest J-factor we consider possible for ω-Cen . For the case of DM annihilating into $\bar{q}q$, there is an allowed range of J-factor values that will be consistent with both constraints on the maximum amount of DM in ω-Cen , and the γ-ray flux. Conversely, the case of DM annihilating into $\mu^+\mu^-$, constraints are more stringent. All of the parameter space is already excluded by CMB, meaning that it will require a very small cross-section and/or a very large J-factor (which translates into very compact objects) to explain the γ-ray flux. Note that taking a p-wave annihilation instead on s-wave relaxes CMB constrains due to the fact that the p-wave DM annihilation does not contribute importantly to the thermal history of the Universe until low redshift.

Despite the fact that only for the $\bar{q}q$ case there is a small window of the allowed parameter space, an assumption that the spectra is produced by multiple contributors can in principle change the values of the mass and cross-section needed to explain the data, possibly lowering the cross section needed to reproduce the photon flux. Recent work assessed the possibility that the γ-ray emission from another globular cluster, 47 Tuc, could be explained by both MSP and DM annihilation. According to [37] the observed photon flux is better fit by a model that includes DM than by a model of MSPs alone, excluding the latter with more than five sigma significance. While [36] argue there is no significant evidence for a DM component if the variance in the spectrum of a population of MSPs is included in the analysis. This stresses the importance of taking into account the uncertainties in the MSP contribution to the photon flux, specially for mixture models (MSPs and DM). In this work, however, we focused on separate limits for each DM annihilation channel in an effort to gain insight not only on possible explanations to ω-Cen 's γ-ray emission, but also to obtain conservative limits on the DM content of ω-Cen under the tidally disrupted dwarf hypothesis.

The results presented were analyzed by taking a 0.2 deg ROI. Nonetheless, for both the MSP and DM hypotheses we repeated our analysis using a 0.15 deg and a 0.5 deg ROI to check for consistency. The posteriors for all three angular regions overlap within 1σ with the three different data sets.

The predicted γ-ray flux for each DM model and for the MSP model is shown in Figure 2, based on the values presented in Tables IV A and IV B. We see that, qualitatively, the three models are a relatively good fit to the data. A quantitative comparison using the AIC factor, shown in the aforementioned tables, leads to the conclusion that the MSP explanation provides a better fit than the DM models. As in [36, 37] a joint analysis with both MSPs and DM could be performed. After an eventual confirmation of a population of MSPs in ω-Cen , they could be included as an additional background in the DM annihilation scenario. In this case, the DM constraints would become much more stringent. Because of ω-Cen 's potentially large J-factor , the DM constraints may eventually be competitive with those from dwarf spheroidal galaxies. To reach this level we also need a better knowledge of the dark matter density distribution within ω-Cen . This can be explored in future dedicated analysis of ω-Cen 's stellar kinematics.

To summarize, here we have addressed for the first time the possibility that the γ-ray emission from ω-Cen can be explained by DM annihilation. Such models are quite constrained. Constraints can also be given in terms of the maximum content of DM in ω-Cen . Further studies of ω-Cen will shed light on the origin of this peculiar system. Dedicated analysis of the J-factor will help narrow down the possibilities for DM to explain the observed γ-ray flux and the confirmation of the existence of MSPs (or other astrophysical sources) will allow stronger constraints on the DM content and properties of ω-Cen .

ACKNOWLEDGEMENTS

This work was partially funded by a UCMEXUS-CONACYT collaborative project and CONACYT project 28689. AXGM acknowledges support from Catedras CONACYT. SP is partly supported by the U.S. Department of Energy grant number de-sc0010107.OV acknowledges support from the PAPIIT-UNAM grant IN112518.

Appendix A: Integrated PSF for nearby point sources

As stated in Section III, to account for the number of events we must consider the instrument response and in particular the information contained in the point spread function (PSF). The energy-dependent probability of detecting a photon within the ROI is computed by integrating over the ROI,

$$\mathrm{PSF}(E) = \int_{\Delta\Omega} \mathrm{PSF}(\theta|E)\, d\Omega, \tag{A1}$$

where θ is the angle between the point within the ROI and the γ-ray source.

For the small angles under consideration we can take the sky as a flat plane and integrate the PSF in rectangular coordinates. The standard integration for ω-Cen is straightforward and has no major complication. However, when we perform the integration for the nearby source, we must integrate its PSF also in a circle centered on ω-Cen , this can be achieved by

$$\mathrm{PSF}(E) = \int_{-\theta}^{\theta} dx \int_{-\sqrt{\theta^2-x^2}}^{\sqrt{\theta^2-x^2}} dy \mathrm{PSF}\left(\sqrt{(D-x)^2+y^2}|E\right), \tag{A2}$$

where θ is radius of the ROI and $D = 0.63^\circ$ is the angular separation between the source and ω-Cen .

Appendix B: Convolution of the Point Spread Function and the J-factor

To compute the differential flux we must convolve the J-profile and the PSF as in Eq. (12). We make use of the very efficient procedure introduced in [69]. Just as in the last section, we take the source to be in a 2D rectangular plane where the angular separation is approximated by the Euclidean distance. The convolution then has to be done through a 2D integral in the xy plane. We compute the convolution very efficiently by going to Fourier space and taking advantage of the circular symmetry of both the J-profile and PSF. Let $(J * \mathrm{PSF})(x, y)$ be denoted by $f(x, y)$. Then

$$f(x,y) = \int dx'dy'\, J(x',y')\, \mathrm{PSF}(x-x', y-y'). \tag{B1}$$

The Fourier transform of f is a function only of the magnitude of the k-vector $\hat{f}(k_x, k_y) = \hat{f}\left(k = \sqrt{k_x^2 + k_y^2}\right)$ and takes the form

$$\begin{aligned}\hat{f}(k) = &\left(\int_0^\infty 2\pi r \frac{dJ}{d\Omega}(r) \jmath_0(kr) dr\right) \\ &\times \left(\int_0^\infty 2\pi r \mathrm{PSF}(r, E) \jmath_0(kr) dr\right),\end{aligned} \tag{B2}$$

where $\jmath_0$ is the Bessel function of zero order and $dJ/d\Omega$ is defined in Eq. 8 (r being the Euclidean approximation to angle θ). The two terms in (B2) (except for a factor of 2π) are the zeroth-order Hankel transforms, which can be performed efficiently using the FFTlog algorithm [58] and the python package `mcfit`. We followed the description of the algorithm described in Ref. [69] to avoid numerical issues when using mcfit and we used the default parameters given by the package functions.

[1] L. L. Watkins, G. van de Ven, M. den Brok, and R. C. E. van den Bosch. Discrete dynamical models of omega Centauri. MNRAS, 436:2598–2615, December 2013.

[2] Laura L. Watkins, Roeland P. van der Marel, Andrea Bellini, and Jay Anderson. Hubble Space Telescope proper motion (HSTPROMO) catalogs of Galactic globular clusters. II. Kinematic profiles and maps. *Astrophys. J.*, 803(1):29, 2015.

[3] Dean E. McLaughlin and Roeland P. van der Marel. Resolved Massive Star Clusters in the Milky Way and its Satellites: Brightness Profiles and a Catalogue of Fundamental Parameters. *Astrophys. J. Suppl.*, 161:304, 2005.

[4] Laura L. Watkins, Roeland P. van der Marel, Andrea Bellini, and Jay Anderson. Hubble Space Telescope Proper Motion (HSTPROMO) Catalogs of Galactic Globular Clusters. III. Dynamical Distances and Mass-to-Light Ratios. ApJ, 812:149, Oct 2015.

[5] Kenji Bekki and John E. Norris. The origin of the double main sequence in omega centauri: helium enrichment due to gas fueling from its ancient host galaxy? *Astrophys. J.*, 637:L109–L112, 2006.

[6] Antonio Sollima, E. Pancino, F. R. Ferraro, M. Bellazzini, O. Straniero, and L. Pasquini. Metallicities, relative ages and kinematics of stellar populations in ive ages and kinematics of stellar populations in omega centauri. *Astrophys. J.*, 634:332–343, 2005.

[7] Seok-Joo Joo and Young-Wook Lee. Star Formation Histories of Globular Clusters with Multiple Populations. I. omega Cen, M22, and NGC 1851. *Astrophys. J.*, 762:36, 2013.

[8] F. D'Antona, A. D'Ercole, A. F. Marino, A. P. Milone, P. Ventura, and E. Vesperini. The oxygen vs. sodium (anti)correlation(s) in omega Cen. *Astrophys. J.*, 736:5, 2011.

[9] Jorge Peñarrubia, Anna Lisa Varri, Philip G. Breen, Annette M. N. Ferguson, and Rubén Sánchez-Janssen. Stellar envelopes of globular clusters embedded in dark minihaloes. MNRAS, 471:L31–L35, October 2017.

[10] Jae-Woo Lee, Young-Woon Kang, Jina Lee, and Young-Wook Lee. Enrichment by supernovae in globular clusters

with multiple populations. *Nature*, 462:480, 2009.

[11] Christian I. Johnson, Catherine A. Pilachowski, R. Michael Rich, and Jon P. Fulbright. A Large Sample Study of Red Giants in the Globular Cluster Omega Centauri (NGC 5139). *Astrophys. J.*, 698:2048–2065, 2009.

[12] S. E. Woosley and T. A. Weaver. The Evolution and Explosion of Massive Stars. II. Explosive Hydrodynamics and Nucleosynthesis. ApJS, 101:181, November 1995.

[13] J. E. Norris, K. C. Freeman, and K. J. Mighell. The Giant Branch of omega Centauri. V. The Calcium Abundance Distribution. ApJ, 462:241, May 1996.

[14] Michael Hilker and Tom Richtler. Omega centauri - a former nucleus of a dissolved dwarf galaxy? new evidence from stroemgren photometry. *Astron. Astrophys.*, 362:895–909, 2000.

[15] Oleg Y. Gnedin, HongSheng Zhao, J. E. Pringle, S. Michael Fall, Mario Livio, and Georges Meylan. The unique history of the globular cluster omega centauri. *Astrophys. J.*, 568:L23–L26, 2002.

[16] Giovanni Carraro and Cesario Lia. On the formation and evolution of the globular cluster omega centauri. *Astron. Astrophys.*, 357:977, 2000.

[17] A. Marcolini, A. Sollima, A. D'Ercole, B. K Gibson, and F. R. Ferraro. Modeling the chemical evolution of Omega Centauri using three-dimensional hydrodynamical simulations. MNRAS, 382:443, 2007.

[18] D. Romano, F. Matteucci, M. Tosi, E. Pancino, M. Bellazzini, F. R. Ferraro, M. Limongi, and A. Sollima. The chemical evolution of Omega Centauri's progenitor system. MNRAS, 376:405–415, 2007.

[19] S.-J. Joo and Y.-W. Lee. Star Formation Histories of Globular Clusters with Multiple Populations. I. ω CEN, M22, and NGC 1851. ApJ, 762:36, January 2013.

[20] S. C. Rey, Y. W. Lee, C. Ree, J. M. Joo, Y. J. Sohn, and A. Walker. Ccd photometry of the globular cluster omega centauri. II. stellar populations and age-metallicity relation. *Astron. J.*, 127:958, 2004.

[21] Michael Fellhauer. Omega-Cen - An Ultracompact dwarf galaxy? *Submitted to: Rev. Mod. Astron.*, 2004.

[22] S. R. Majewski, R. J. Patterson, D. I. Dinescu, W. Y. Johnson, J. C. Ostheimer, W. E. Kunkel, and C. Palma. Omega Centauri: Nucleus of a Milky Way Dwarf Spheroidal? In *35th Liege International Astrophysics Colloquium on the Galactic Halo: from Globular Clusters to Field Stars Liege, Belgium, July 5-8, 1999*, 1999.

[23] H. Zinnecker, C. J. Keable, J. S. Dunlop, R. D. Cannon, and W. K. Griffiths. The Nuclei of Nucleated Dwarf Elliptical Galaxies - are they Globular Clusters? In Jonathan E. Grindlay and A. G. Davis Philip, editors, *The Harlow-Shapley Symposium on Globular Cluster Systems in Galaxies*, volume 126 of *IAU Symposium*, page 603, Jan 1988.

[24] T. Tsuchiya, V. I. Korchagin, and D. I. Dinescu. Disruption of a dwarf galaxy under strong shocking: the origin of ω Centauri. MNRAS, 350:1141–1151, May 2004.

[25] Mario Mateo. Dwarf galaxies of the Local Group. *Ann. Rev. Astron. Astrophys.*, 36:435–506, 1998.

[26] Rodrigo Ibata, Michele Bellazzini, Khyati Malhan, Nicolas Martin, and Paolo Bianchini. Identification of the Long Stellar Stream of the Prototypical Massive Globular Cluster Omega Centauri. *arXiv:1902.09544*, Feb 2019.

[27] M. Cappellari, R. M. McDermid, K. Alatalo, L. Blitz, M. Bois, F. Bournaud, M. Bureau, A. F. Crocker, R. L. Davies, T. A. Davis, P. T. de Zeeuw, P.-A. Duc, E. Emsellem, S. Khochfar, D. Krajnović, H. Kuntschner, P.-Y. Lablanche, R. Morganti, T. Naab, T. Oosterloo, M. Sarzi, N. Scott, P. Serra, A.-M. Weijmans, and L. M. Young. Systematic variation of the stellar initial mass function in early-type galaxies. *Nature.*, 484(12):4, jun 2012.

[28] N. Aghanim et al. Planck 2018 results. VI. Cosmological parameters. *arXiv:1807.06209*, 2018.

[29] A. A. Abdo et al. Fermi LAT Search for Photon Lines from 30 to 200 GeV and Dark Matter Implications. *Phys. Rev. Lett.*, 104:091302, 2010.

[30] A. A. Abdo et al. Constraints on Cosmological Dark Matter Annihilation from the Fermi-LAT Isotropic Diffuse Gamma-Ray Measurement. *JCAP*, 1004:014, 2010.

[31] M. Ackermann et al. Fermi LAT Search for Dark Matter in Gamma-ray Lines and the Inclusive Photon Spectrum. *Phys. Rev.*, D86:022002, 2012.

[32] A population of gamma-ray emitting globular clusters seen with the Fermi Large Area Telescope. *Astron. Astrophys.*, 524:A75, 2010.

[33] Simon Henleywillis, Adrienne M. Cool, Daryl Haggard, Craig Heinke, Paul Callanan, and Yue Zhao. A Deep X-ray Survey of the Globular Cluster Omega Centauri. 2018.

[34] S. Profumo. *An Introduction to Particle Dark Matter*. Advanced textbooks in physics. World Scientific, 2017.

[35] Jan Conrad and Olaf Reimer. Indirect dark matter searches in gamma and cosmic rays. *Nature Phys.*, 13(3):224–231, 2017.

[36] Richard Bartels and Thomas Edwards. Comment on "Understanding the γ-ray emission from the globular cluster 47 Tuc: evidence for dark matter?". *arXiv:1807.08800*, 2018.

[37] Anthony M. Brown, Thomas Lacroix, Sheridan Lloyd, Cline Bhm, and Paula Chadwick. Understanding the γ-ray emission from the globular cluster 47 Tuc: evidence for dark matter? *Phys. Rev.*, D98(4):041301, 2018.

[38] The Fermi-LAT collaboration. Fermi Large Area Telescope Fourth Source Catalog. *arXiv:1902.10045*, 2019.

[39] M. Wenger, F. Ochsenbein, D. Egret, P. Dubois, F. Bonnarel, S. Borde, F. Genova, G. Jasniewicz, S. Laloë, S. Lesteven, and R. Monier. The SIMBAD astronomical database. The CDS reference database for astronomical objects. A&AS, 143:9–22, April 2000.

[40] A. A. Abdo et al. A Population of Gamma-Ray Millisecond Pulsars Seen with the Fermi Large Area Telescope. *Science*, 325(5942):848–852, 2009.

[41] Dan Hooper and Tim Linden. The Gamma-Ray Pulsar Population of Globular Clusters: Implications for the GeV Excess. *JCAP*, 1608(08):018, 2016.

[42] Ilias Cholis, Dan Hooper, and Tim Linden. A New Determination of the Spectra and Luminosity Function of Gamma-Ray Millisecond Pulsars. *arXiv:1407.5583*, 2014.

[43] F. Acero et al. Fermi Large Area Telescope Third Source Catalog. *Astrophys. J. Suppl.*, 218(2):23, 2015.

[44] Daniel Foreman-Mackey, David W. Hogg, Dustin Lang, and Jonathan Goodman. emcee: The MCMC Hammer. *Publications of the Astronomical Society of the Pacific*, 125(925):306, Mar 2013.

[45] Farhan Feroz and M. P. Hobson. Multimodal nested sampling: an efficient and robust alternative to MCMC methods for astronomical data analysis. MNRAS, 384:449, 2008.

[46] J. Buchner, A. Georgakakis, K. Nandra, L. Hsu, C. Rangel, M. Brightman, A. Merloni, M. Salvato,

J. Donley, and D. Kocevski. X-ray spectral modelling of the AGN obscuring region in the CDFS: Bayesian model selection and catalogue. A&A, 564:A125, April 2014.

[47] Alex Geringer-Sameth, Savvas M. Koushiappas, and Matthew Walker. Dwarf galaxy annihilation and decay emission profiles for dark matter experiments. *Astrophys. J.*, 801(2):74, 2015.

[48] Louis E. Strigari, Savvas M. Koushiappas, James S. Bullock, and Manoj Kaplinghat. Precise constraints on the dark matter content of Milky Way dwarf galaxies for gamma-ray experiments. *Phys. Rev.*, D75:083526, 2007.

[49] V. Bonnivard et al. Dark matter annihilation and decay in dwarf spheroidal galaxies: The classical and ultrafaint dSphs. MNRAS, 453(1):849–867, 2015.

[50] Kevork N. Abazajian and Manoj Kaplinghat. Detection of a Gamma-Ray Source in the Galactic Center Consistent with Extended Emission from Dark Matter Annihilation and Concentrated Astrophysical Emission. *Phys. Rev.*, D86:083511, 2012. [Erratum: Phys. Rev.D87,129902(2013)].

[51] M. Ackermann et al. The Fermi Galactic Center GeV Excess and Implications for Dark Matter. *Astrophys. J.*, 840(1):43, 2017.

[52] Gregory D. Martinez. A robust determination of Milky Way satellite properties using hierarchical mass modelling. MNRAS, 451(3):2524–2535, Aug 2015.

[53] A. Bellini, J. Anderson, R. P. van der Marel, L. L. Watkins, I. R. King, P. Bianchini, J. Chanamé, R. Chandar, A. M. Cool, F. R. Ferraro, H. Ford, and D. Massari. Hubble Space Telescope Proper Motion (HSTPROMO) Catalogs of Galactic Globular Clusters. I. Sample Selection, Data Reduction, and NGC 7078 Results. ApJ, 797:115, December 2014.

[54] Laura L. Watkins, Glenn van de Ven, Mark den Brok, and Remco C. E. van den Bosch. Discrete dynamical modelling of omega Centauri. MNRAS, 436:2598, 2013.

[55] Kenji Bekki and K. C. Freeman. Formation of omega Centauri from an ancient nucleated dwarf galaxy in the young Galactic disc. MNRAS, 346:L11, 2003.

[56] Anatoly Klypin, Gustavo Yepes, Stefan Gottlober, Francisco Prada, and Steffen Hess. Multidark simulations: the story of dark matter halo concentrations and density profiles. MNRAS, 457:4340, 4 2016.

[57] Sergey V. Pilipenko, Miguel A. Snchez-Conde, Francisco Prada, and Gustavo Yepes. Pushing down the low-mass halo concentration frontier with the lomonosov cosmological simulations. MNRAS, 472:4918, 2017.

[58] A. J. S. Hamilton. Uncorrelated modes of the nonlinear power spectrum. MNRAS, 312:257–284, 2000.

[59] Raniere de Menezes, Fabio Cafardo, and Rodrigo Nemmen. Milky Way globular clusters in gamma-rays: analyzing the dynamical formation of millisecond pulsars. *arXiv:1811.06957*, 2018.

[60] Gerard Jungman, Marc Kamionkowski, and Kim Griest. Supersymmetric dark matter. *Phys. Rept.*, 267:195–373, 1996.

[61] John McDonald. Gauge singlet scalars as cold dark matter. *Phys. Rev.*, D50:3637–3649, 1994.

[62] M. S. Boucenna and S. Profumo. Direct and Indirect Singlet Scalar Dark Matter Detection in the Lepton-Specific two-Higgs-doublet Model. *Phys. Rev.*, D84:055011, 2011.

[63] Stefano Profumo, Lorenzo Ubaldi, and Carroll Wainwright. Singlet Scalar Dark Matter: monochromatic gamma rays and metastable vacua. *Phys. Rev.*, D82:123514, 2010.

[64] Stefano Profumo. Astrophysical Probes of Dark Matter. In *Proceedings, Theoretical Advanced Study Institute in Elementary Particle Physics: Searching for New Physics at Small and Large Scales (TASI 2012): Boulder, Colorado, June 4-29, 2012*, pages 143–189, 2013.

[65] Richard Bartels, Daniele Gaggero, and Christoph Weniger. Prospects for indirect dark matter searches with MeV photons. *JCAP*, 1705(05):001, 2017.

[66] Lars Bergstrom, Piero Ullio, and James H. Buckley. Observability of gamma-rays from dark matter neutralino annihilations in the Milky Way halo. *Astropart. Phys.*, 9:137–162, 1998.

[67] Tracy R. Slatyer. Energy Injection And Absorption In The Cosmic Dark Ages. *Phys. Rev.*, D87(12):123513, 2013.

[68] Gary Steigman, Basudeb Dasgupta, and John F. Beacom. Precise Relic WIMP Abundance and its Impact on Searches for Dark Matter Annihilation. *Phys. Rev.*, D86:023506, 2012.

[69] Alex Geringer-Sameth, Savvas M. Koushiappas, and Matthew G. Walker. Comprehensive search for dark matter annihilation in dwarf galaxies. *Phys. Rev.*, D91(8):083535, 2015.